

PAPER • OPEN ACCESS

Development of a Novel DEMO divertor target: spiral plate module

To cite this article: N R Schwartz *et al* 2021 *Phys. Scr.* **96** 124027

View the [article online](#) for updates and enhancements.

You may also like

- [ERO modeling and analysis of tungsten erosion and migration from a toroidally symmetric source in the DIII-D divertor](#)
J. Guterl, T. Abrams, C.A. Johnson et al.
- [Plasma detachment in divertor tokamaks](#)
A W Leonard
- [Three-dimensional modeling of plasma edge transport and divertor fluxes during application of resonant magnetic perturbations on ITER](#)
O. Schmitz, M. Becoulet, P. Cahyna et al.



PAPER

OPEN ACCESS

RECEIVED
20 May 2021

REVISED
12 August 2021

ACCEPTED FOR PUBLICATION
9 September 2021

PUBLISHED
22 September 2021

Original content from this work may be used under the terms of the [Creative Commons Attribution 4.0 licence](#).

Any further distribution of this work must maintain attribution to the author(s) and the title of the work, journal citation and DOI.



Development of a Novel DEMO divertor target: spiral plate module

N R Schwartz , J R Nicholas, Z J Jackson and P T Ireland

Osney Thermofluids Institute, Southwell Building, University of Oxford, Department of Engineering Science, Osney Mead, Oxfordshire, OX2 0ES, United Kingdom

E-mail: nick.schwartz@eng.ox.ac.uk

Keywords: divertor, modular, target, DEMO, CFD, tungsten

Abstract

In DEMO, the divertor must endure steady state loads of 10 MW m^{-2} and transient thermal cycling up to 20 MW m^{-2} . A novel divertor target, termed the Spiral Plate Module (SPM) and designed to meet these loads, was initially optimized by a one-dimensional, steady-state model. The best design was a trade-off between the wall overhear (τ_s)—a figure of merit for cooling performance and the pumping ratio (η_p)—a comparison of the pressure drop and the incident heat flux on a target surface. A three-dimensional, steady-state, conjugate heat transfer study showed significant correlation to the one-dimensional model. Compared to other divertor target concepts, the SPM achieved the lowest wall overhear of any target design. The hydraulic performance was also on par with comparable designs, demonstrating a very low pumping ratio. This novel, modular divertor target could be used in future fusion power plants to effectively cool the plasma facing components with low pressure drop.

Introduction

The body of innovative work on thermal exhaust concepts for divertors is diverse in many ways. Much of the progress has focused on minimizing the heat flux by gas puffing [1–3], beam injection [4], and various divertor configurations [5]. In parallel, helium, water, and liquid metal coolants have all been tested in a variety of configurations and geometries. Indeed, a medley of enhancement methods for increasing the heat transfer coefficient, h , have been conceptualized [6] and tested, such as hypervaportrons [7], swirl tapes [8], porous flow [9], microfins [10], jet impingement [11–13], and magnetohydrodynamic effects [14] to name a few.

Modular designs, like the high-pressure jet cascade (HPJC) of Nicholas *et al* [13], offer several benefits over integrated, channel-flow designs such as the ITER-like W monoblock [15]. Modularity allows for user-specified control of mass flow rates to different areas of the divertor. Because the heat flux can vary from an average ~ 5 up to a peak of $\sim 20 \text{ MW m}^{-2}$ [16], it is beneficial to control the mass flow rate to match the heat flux profile.

One of the negatives of impinging jets is the pressure drop associated with the stagnation point. Yet, impinging jets offer some of the best heat transfer capabilities because of the thin boundary layer that forms upon impact. The author has designed a novel divertor target that aims to achieve high heat transfer coefficients—like those of impinging jets—while maintaining a low pressure drop. This design is based on the cooling mechanism in a concept for producing neutrons in a radiation-based cancer treatment known as Boron-Neutron Capture Therapy [17]. This new design was termed the Spiral Plate Module (SPM).

Conceptual design

The general shape of the module was chosen to be a hexagon to maximize areal packing density. The design consists of four major components (figure 1): the target plate, swirl plate, backing, and housing. The critical portion of the design is contained in the spiral plate, as convective heat transfer and pressure drop can be considered negligible elsewhere.

The heat flux strikes the fully tungsten target plate. The target plate can withstand the high temperatures and neutron flux present during steady-state operation of DEMO. Coolant enters and exits through channels in the

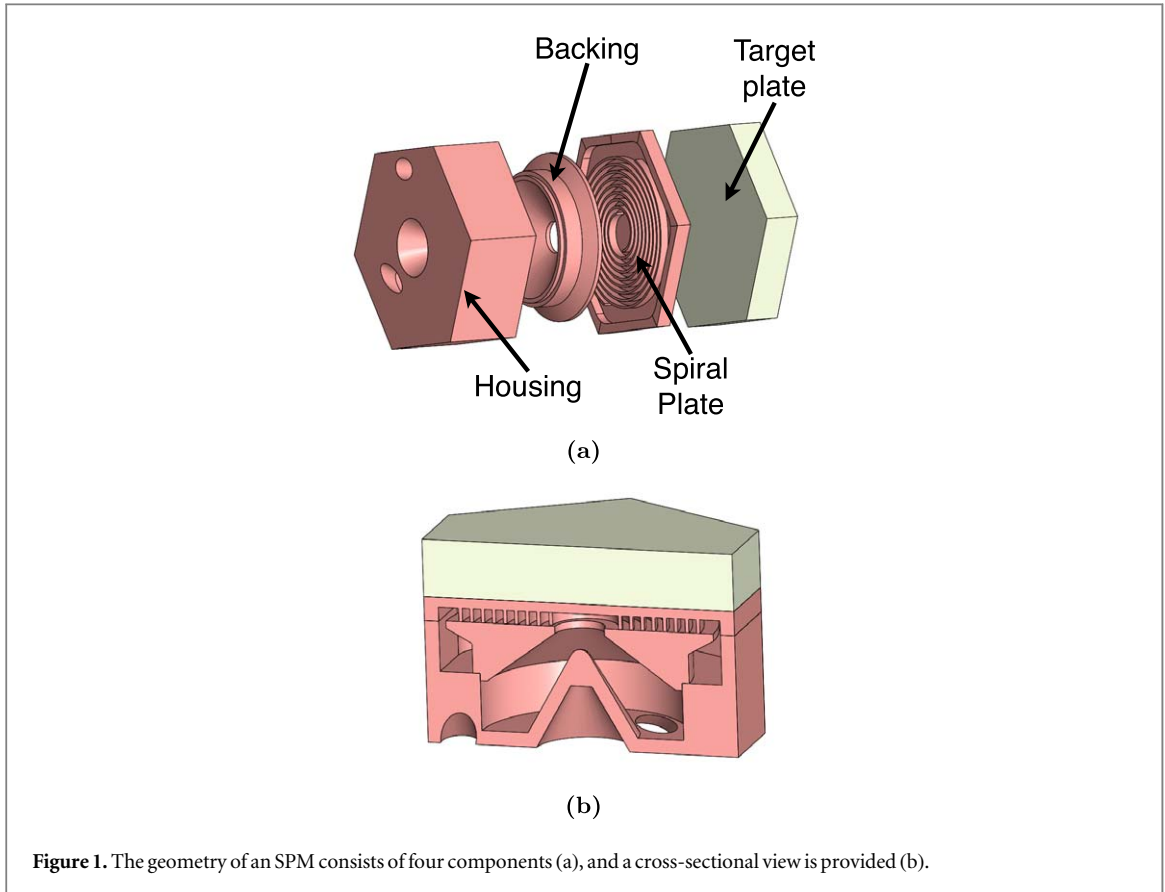


Figure 1. The geometry of an SPM consists of four components (a), and a cross-sectional view is provided (b).

housing. The design directs coolant towards the spiral plate by inducing a vortex. The vortex flow strikes the spiral plate, which directs the flow in several spiral channels with a non-circular cross-section. The backing separates the inlet and outlet. A seal may be formed by diffusion bonding the backing to the spiral plate and housing. The backing also prevents flow from one spiral channel from flowing into another in the radial direction.

1D numerical optimization

A one-dimensional model was created in MATLAB to optimize the geometry. The following assumptions were made: (1) The flow is one-dimensional along the streamwise direction; (2) the flow is single-phase; (3) there is negligible contact resistance between the target and spiral plates; (4) the curved channels range from the center of the hexagon to its apothem; (5) the mass flow rate is divided equally among n spiral channels; and (6) each channel is exposed to an equal amount of heat flux per unit area.

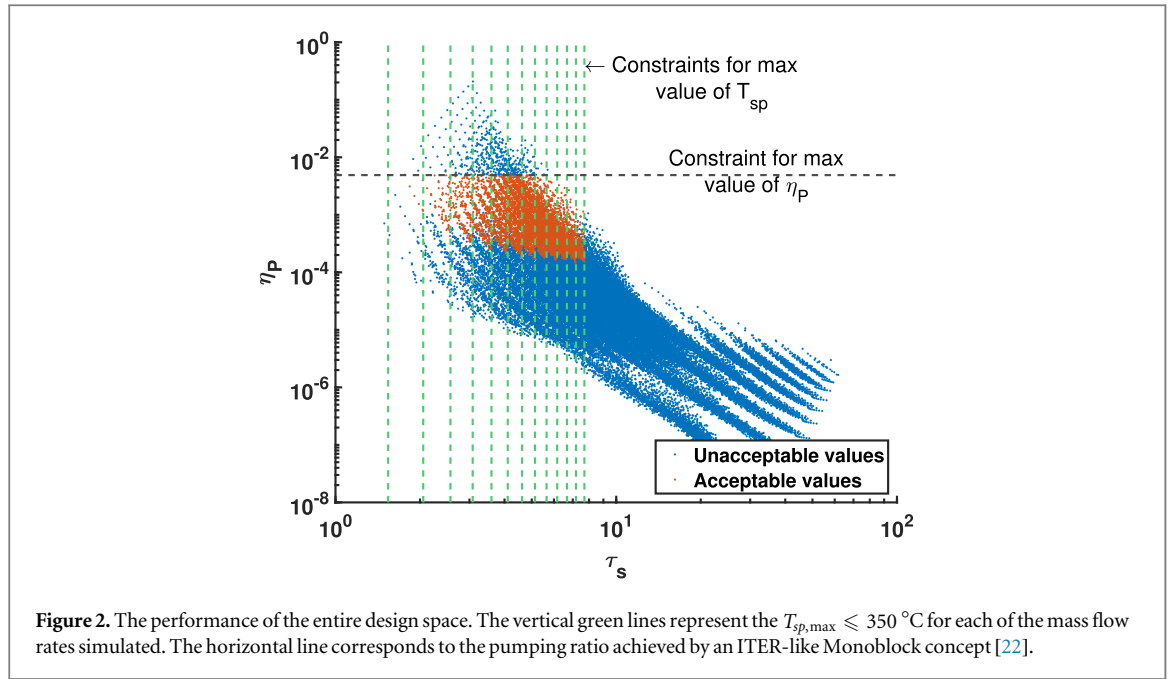
Water was used as the coolant, and the liquid and vapor properties were taken from the NIST tables. CuCrZr was chosen as the swirl plate material and tungsten as the target plate material, the properties of which were taken from appendix A of the ITER SDC-IC.

The maximum allowable temperature of the spiral plate, $T_{sp,max}$, was set to 350 °C per [18]. Above this temperature thermal fatigue/creep becomes apparent; although irradiated material will have worse thermomechanical performance [19], those effects were not considered. The tungsten target plate is limited by an operational window between 500 °C and 1300 °C that becomes even smaller with irradiation [20]. DBTT determines the lower limit, and recrystallization/creep the upper.

The pumping power is defined by the mass flow rate (\dot{m}), the pressure drop (ΔP), and the fluid density (ρ_f) as:

$$\dot{P} = \frac{\dot{m}\Delta P}{\rho_f} \quad (1)$$

The pumping ratio, η_p , is an important parameter to determine whether or not the pressure drop is too large based on the total incident heat flux, \dot{Q} , where A_t is simply the area of the target:



$$\eta_p = \frac{\dot{P}}{\dot{Q}} = \frac{\dot{P}}{A_t \dot{q}} \quad (2)$$

For He-cooled divertors, this ratio must not exceed 10%, according to [21]. However, the value for η_p is typically significantly lower when water is used as the coolant. For example, the ITER-like Monoblock concept has a pumping ratio of 0.0049 [22]. Therefore, this water-cooled design must meet or exceed the hydraulic performance of the ITER-like design.

The wall overhear, τ_s , was then defined using the maximum heat sink temperature and the coolant inlet temperature, T_{ci} [22]. For a specific dimensionless mass flow (m^*), an efficient cooling system will minimize τ_s ,

$$\tau_s = \frac{\dot{m}c_p(T_{sp,max} - T_{ci})}{\dot{Q}} = \frac{\text{max heat extraction}}{\text{actual heat removal}} \quad (3)$$

For the dimensionless mass flow rate, the thickness of the heat sink (t_{sp}), the fluid specific heat (c_p), and the spiral plate thermal conductivity (k_{sp}), were used.

$$m^* = \frac{\dot{m}c_p t_{sp}}{k_{sp} A_t} = \frac{\text{thermal fluid capacity flux}}{\text{solid thermal conductance}} \quad (4)$$

Figure 2 presents the results for the overall performance metrics over the entire design space. Choosing a single ‘best’ design was a trade-off between low pumping ratios and high wall overhear for a given mass flow rate. Typically, a lower pumping ratio corresponds to a larger wall overhear, and vice-versa. More importance was placed on the cooling capabilities (and thus τ_s) than the pumping ratio because avoiding critical heat flux is imperative to protect surrounding hardware and the users.

Computational validation

Model creation

Having selected a geometry, a conjugate heat transfer study in ANSYS CFX was performed. Water was modeled using the IAPWS-97 library in CFX. A reference pressure of 20 MPa was chosen based on the HPJC concept [13]. The CuCrZr and W armor properties were taken at a reference temperature of 300 °C and 900 °C, respectively, from the ITER SDC-IC

A constant, uniform heat flux of 10 MW m⁻² was applied to the top surface of the target plate, and all other external surfaces were adiabatic. The fluid inlet was given a mass flow rate boundary condition with a temperature of 150 °C, which meets the lower limit for CuCrZr embrittlement [16, 23].

All results achieved root-mean-squared residuals lower than 5×10^{-5} and global imbalances below 1%. The mesh was refined to four different levels, and given the results from global and local comparisons, a mesh with 11.3 million fluid cells was chosen as the reference mesh, as further refinement would have had a negligible effect on the results.

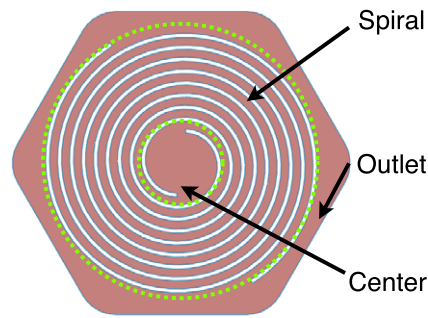


Figure 3. Considering local phenomenon, there were primarily three regions of interest: the center, spiral, and outlet.

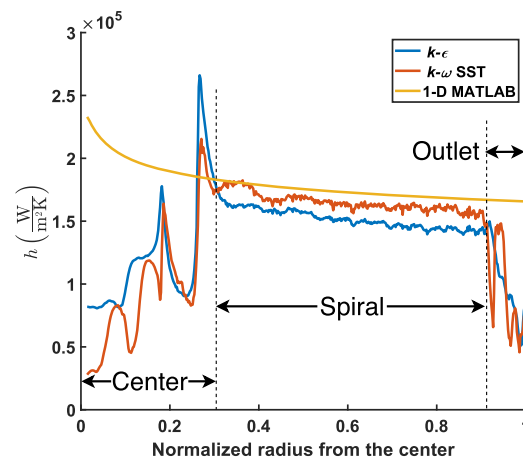


Figure 4. Variation of local heat transfer coefficient along the normalized radius.

Table 1. Comparison of the CFD studies on the SPM to the 1D model in MATLAB. Mass flow rates for both $k-\epsilon$ and $k-\omega$ studies are such that the maximum temperature of the CuCrZr heat sink was nominally 350 °C.

Design	τ_s	m^*	η_p	Re_A
SPM (1D)	2.40	0.675	4.6E-3	8.54E3
SPM ($k-\epsilon$)	3.34	0.675	3.3E-3	8.54E3
SPM ($k-\omega$)	3.31	0.675	3.2E-3	8.54E3

Reference case

Two reference simulations were performed with both the scalable $k-\epsilon$ and the $k-\omega$ SST with automatic wall treatment. Mesh in the fully resolved $k-\omega$ SST model were grown such that $y^+ < 2$. The y^+ values were confirmed by obtaining the average value on the heat flux surface; they were 97 and 1.15 for the $k-\epsilon$ and $k-\omega$ models, respectively.

Results for both reference meshes and the one-dimensional model are outlined in table 1. The value of the ΔP used to calculate η_p was determined by calculating the mass flow averaged relative pressure at the inlet (given that the outlet had a zero-pressure condition).

There were three regions of interest on the heat flux surface of the fluid figure 3—the center (where the swirling flow first strikes the spiral plate), the spiral (where the flow is channeled through the spirals), and the outlet (where the flow exits the channels and moves around the outside toward the outlet).

The 1D model does not account for the initial swirling flow that strikes the heat sink surface. Instead, it assumes that there is no thermohydraulic entrance length and the spiral channel begins at the center of the target. For this reason, the pressure drop is higher in this region in the 1D model, but the heat transfer coefficient is actually over-predicted. These two conclusions would lead to a lower τ_s , but higher η_p , in the 1D model.

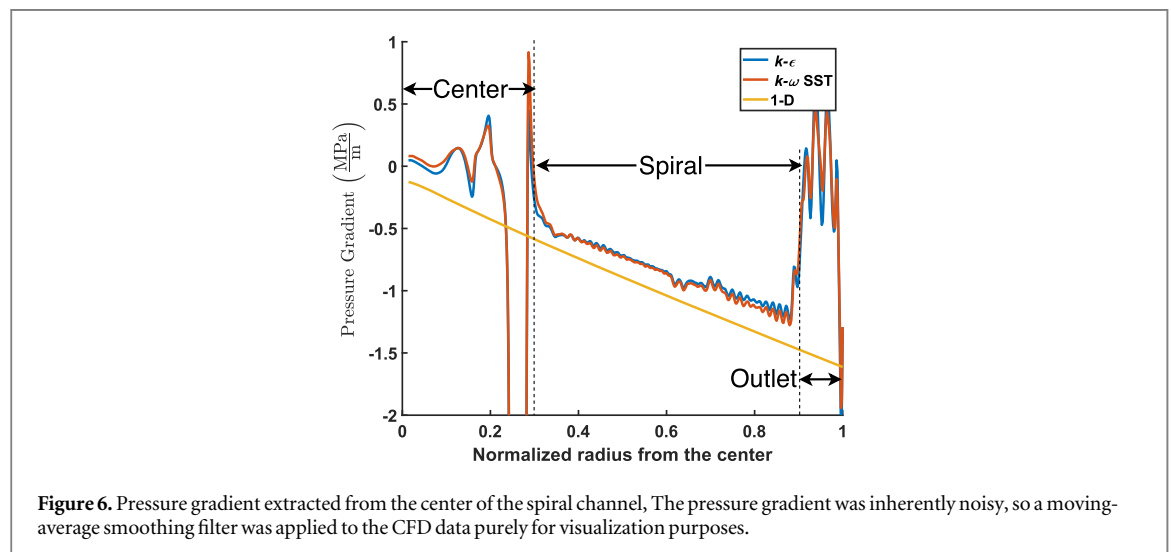
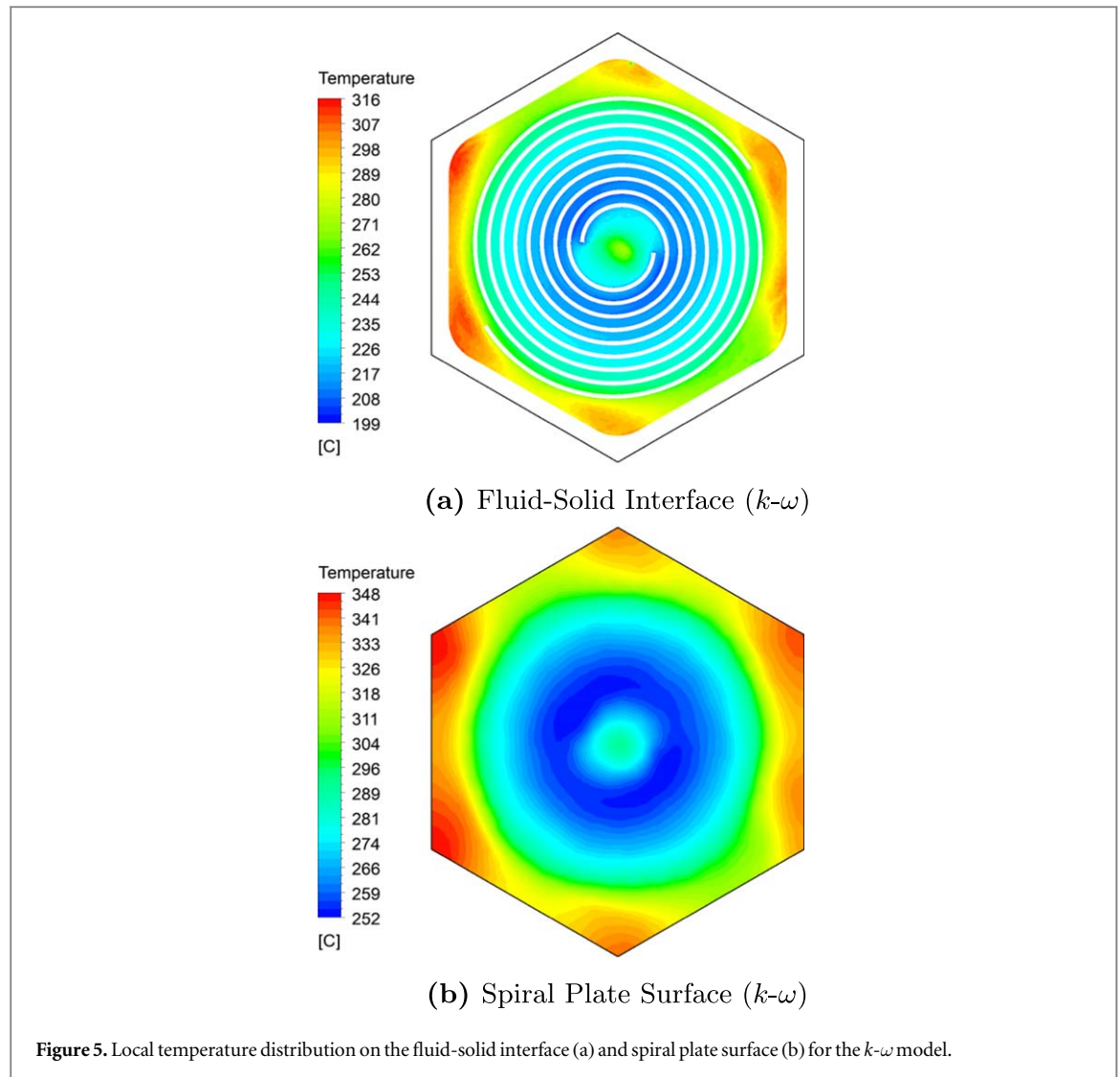
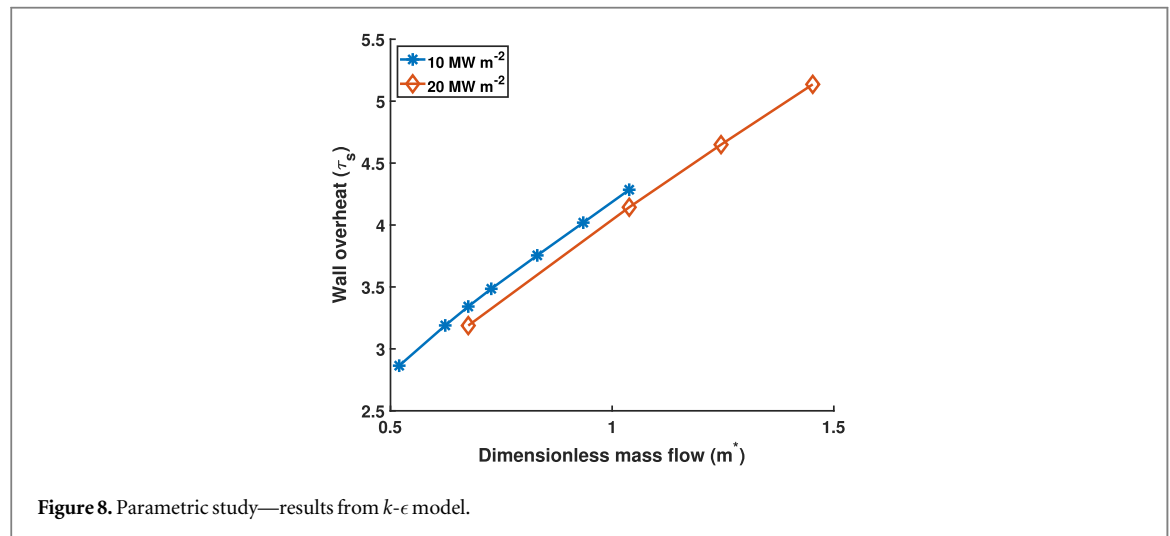
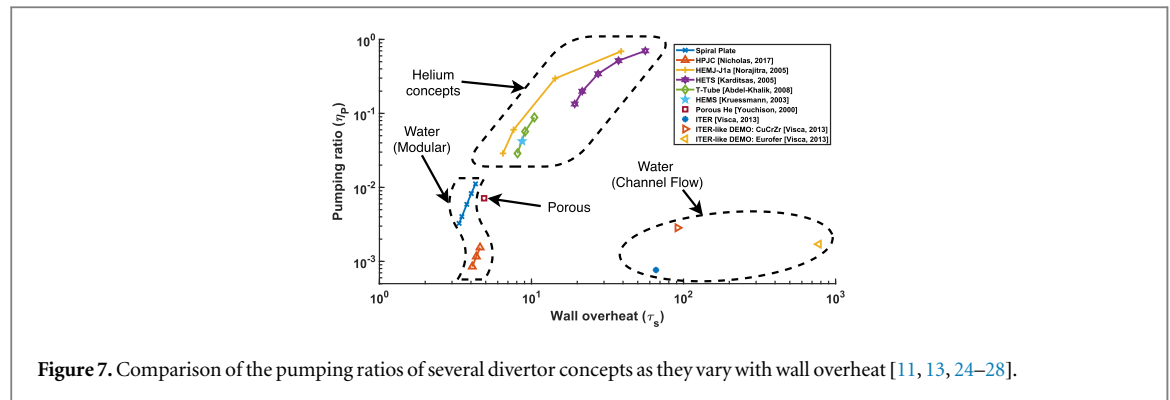


Figure 4 shows a comparison of the two reference simulations and 1D model. In this spiral section, $k-\omega$ predicts a higher h likely because the mesh fully resolves the boundary layer, whereas $k-\epsilon$ only models the boundary layer through wall functions. The 1D model does a poor job of predicting h in the center and outlet region, but this was expected because it treated entire geometry as a spiral channel flow. On the other hand, in the spiral region, the 1D model shows good agreement with $k-\omega$, with an average 5.2% difference.



The temperature distributions on the fluid-solid interface and heat sink are shown in figure 5. The $k-\omega$ model predicted a peak solid temperature of 348 °C, which differs by only 0.6% from the nominal value.

The minimum temperature of the fluid-solid interface was greater than 190 °C, meaning that the inlet temperature could be reduced to match the lower limit of 150 °C for CuCrZr embrittlement [16, 23]. By lowering the inlet temperature, the peak temperature on the solid could also be reduced. Additionally, the maximum solid temperature occurred in the corners of the module. These local maxima could be addressed by increasing the number of channels or extending the spiral channels farther out radially.

The local pressure gradient was considered in detail in figure 6. Visually, the $k-\epsilon$ and $k-\omega$ models seem to match quite well, and in fact, there was only a 4.7% average difference between the pressure gradients of each in the spiral region. The 1D model predicted a higher pressure drop, and the pressure gradient was larger in magnitude, with an average difference of 29% in the spiral region when compared to the $k-\omega$ model.

Although the entrance section, where there was a large pressure gradient, is relatively short, it contributed substantially to the overall 0.7 MPa pressure drop (36%). The magnitude of the gradient in this region could be improved by changing the geometry to gradually ease the flow into the spiral channel, as opposed to ‘squeezing’ the coolant all at once.

Divertor target design comparison

A useful way to visualize performance is simultaneously comparing the pumping ratio and wall overhear (figure 7). A good design will have both low τ_s and η_p . Channel flow concepts like the ITER-like design have significantly higher wall overhear because the mass flow rate per unit area must be large to limit the CuCrZr temperature to 350 °C. Even though there is a relatively large pressure drop that is associated with modular designs like the SPM and HPJC, the heat removal rate is significantly improved over channel flow. For this reason, the pumping ratio of modular, water-based designs is usually smaller or comparable to the ITER-like design.

The SPM achieves the lowest wall overhear of any design, but not the lowest pumping ratio. Nonetheless, the pumping power is still less than 1% of the incident heat flux, which is considered very good performance.

Significant progress has been made to minimize the maximum heat flux (some methods mentioned in the Introduction). However, some devices still produce steady-state fluxes in excess of 10 MW m^{-2} , and off-normal disruptions can produce fluxes up to 20 MW m^{-2} . Therefore, a parametric study was performed for different mass flow rates and incident fluxes (figure 8). Wall overheat was linearly related to \dot{m}^* , as expected from (3), but was nearly constant (within 5% difference) for different heat fluxes, which is likely due to a linear increase in the maximum spiral plate temperature with increasing flux.

Conclusions

A novel divertor target design was created—the Spiral Plate Module (SPM)—to meet the intense thermal loads predicted in DEMO. The chosen geometry was optimized through a 1D model, based on the pumping ratio and wall overheat. A CFD study was then performed and showed good agreement on local variations of h and the pressure gradient in the spiral region. The spiral plate design had the lowest wall overheat of all concepts considered while satisfying all the temperature requirements for both the tungsten armor and CuCrZr heat sink. The pumping power necessary to cool the module was less than 1% of the incident heat flux.

Data availability statement

The data that support the findings of this study are available upon reasonable request from the authors.

ORCID iDs

N R Schwartz  <https://orcid.org/0000-0002-9684-6435>

References

- [1] Gruber O et al 1995 *Phys. Rev. Lett.* **74** 4217–20
- [2] Loarte A et al 1998 *Nucl. Fusion* **38** 331–71
- [3] Fenstermacher M et al 1999 *Plasma Phys. Controlled Fusion* **41** A345
- [4] Gao J et al 2017 *Nuclear Materials and Energy* **12** 1025–9 Proceedings of the 22nd International Conference on Plasma Surface Interactions 2016, 22nd PSI
- [5] Reimerdes H et al 2020 *Nucl. Fusion* **60** 066030
- [6] Norajitra P, Abdel-Khalik S I, Giancarli L M, Ihli T, Janeschitz G, Malang S, Mazul I V and Sardain P 2008 *Fusion Eng. Des.* **83** 893–902 Proceedings of the Eight International Symposium of Fusion Nuclear Technology
- [7] Wang Z, Song Y and Huang S 2012 *Fusion Eng. Des.* **87** 868–71 10th International Symposium on Fusion Nuclear Technology (ISFNT-10)
- [8] Suzuki S, Ezato K, Seki Y, Mohri K, Yokoyama K and Enoda M 2012 *Fusion Eng. Des.* **87** 845–52 10th International Symposium on Fusion Nuclear Technology (ISFNT-10)
- [9] Rosenfeld J, Lindemuth J, North M, Watson R, Youchison D and Goulding R 1997 Evaluation of porous media heat exchangers for fusion applications *Fusion Technology* ed C Varandas and F Serra (Oxford: Elsevier) pp 487–90
- [10] Baxi C and Wong C 2000 *Fusion Eng. Des.* **51**–52 319–324
- [11] Norajitra P, Giniyatulin R, Holstein N, Ihli T, Krauss W, Kruessmann R, Kuznetsov V, Mazul I, Ovchinnikov I and Zeep B 2005 *Fusion Eng. Des.* **75–79** 307–11 Proceedings of the 23rd Symposium of Fusion Technology
- [12] Raffray A, Malang S and Wang X 2009 *Fusion Eng. Des.* **84** 1553–7 Proceeding of the 25th Symposium on Fusion Technology
- [13] Nicholas J R, Ireland P T, Hancock D and Robertson D 2017 *Fusion Sci. Technol.* **72** 566–73
- [14] Ruzic D, Xu W, Andruczyk D and Jaworski M 2011 *Nucl. Fusion* **51** 102002
- [15] You J et al 2021 *J. Nucl. Mater.* **544** 152670
- [16] You J et al 2016 *Nuclear Materials and Energy* **9** 171–6
- [17] Bayanov B, Belov V and Taskaev S 2006 *J. Phys. Conf. Ser.* **41** 460–5
- [18] You J H 2015 *Nucl. Fusion* **55** 113026
- [19] Singh B, Tähtinen S, Moilanen P, Jacquet P, Dekeyser J, Edwards D, Li M and Stubbins J 2007 Fatigue deformation behaviour of a CuCrZr alloy: COFAT 1 *Ris J-R* 1571 (https://inis.iaea.org/collection/NCLCollectionStore/_Public/38/083/38083095.pdf)
- [20] Bazylev B and Fetzer R 2014 The quantification of the key physics parameters for the demo fusion power reactor and analysis of the reactor relevant physics issues *KIT Scientific Reports* 7661 Karlsruhe Institut für Technologie (KIT) (<https://d-nb.info/1067484795/34>)
- [21] Rimza S, Satpathy K, Khirwadkar S and Velusamy K 2014 Numerical studies on helium cooled divertor finger mock up with sectorial extended surfaces *Fusion Eng. Des.* **89** 2647–58
- [22] Nicholas J 2017 Heat transfer for fusion power plant divertors *PhD Thesis* University of Oxford
- [23] Zhang K, Gaganidze E and Gorley M 2019 Development of the material property handbook and database of CuCrZr *Fusion Engineering and Design* **144** 148–153
- [24] Pizzuto A, Karditsas P J, Nardi C and Papastergiou S 2005 *Fusion Eng. Des.* **75–79** 481–4 Proceedings of the 23rd Symposium of Fusion Technology
- [25] Abdel-Khalik S, Crosatti L, Sadowski D, Shin S, Weathers J, Yoda M and Team A 2008 *Fusion Sci. Technol.* **54** 864–77
- [26] Diegele E, Krüssmann R, Malang S, Norajitra P and Rizzi G 2003 *Fusion Engineering and Design—FUSION ENG DES* **66** 383–7
- [27] Youchison D L, North M T, Lindemuth J E, McDonald J M and Lutz T J 2000 *Fusion Eng. Des.* **49–50** 407–15
- [28] Visca E, Crescenzi F, Moriani A, Puma A L, Richou M and Roccella S 2013 Assessment of an iter-like water-cooled divertor for demo *IEEE 25th Symposium on Fusion Engineering (SOFE)* 1–6